The electric double layer at metal-water interfaces revisited based on a charge polarization scheme

Sung Sakong[1,*] and Axel Groß[1,2,†]

[1] *Institute of Theoretical Chemistry, Ulm University, 89069 Ulm, Germany*
[2] *Helmholtz Institute Ulm (HIU), Electrochemical Energy Storage, 89069 Ulm, Germany*

The description of electrode-electrolyte interfaces is based on the concept of the formation of an electric double layer. This concept was derived from continuum theories extended by introducing point charge distributions. Based on ab initio molecular dynamics simulations, we analyze the electric double layer in an approach beyond the point charge scheme by instead assessing charge polarizations at electrochemical metal-water interfaces from first principles. We show that the atomic structure of water layers at room temperature leads to an oscillatory behavior of the averaged electrostatic potential. We address the relation between the polarization distribution at the interface and the extent of the electric double layer and subsequently derive the electrode potential from the charge polarization.

I. INTRODUCTION

There is a growing demand for advanced electrochemical devices for energy storage and energy conversion, for example for electrical vehicles or smart devices [1, 2]. Despite of the technological progress, some fundamental aspect of electrochemistry derived from macroscopic electrostatic theory are still not satisfactorily characterized on the explicit atomistic level. The electric double layer at electrochemical interfaces is typically described by the Helmholtz layer at charged surfaces and extensions based on point charge distributions [3–7]. The electrode potential can accordingly been derived from the capacitance at an electrode. There have been numerous attempts to improve the description [8–10], but it is fair to say that the theoretical treatment of the double layer is still incomplete. This is mainly due to the fact that a correct description of the electric double layer requires a realistic electron distribution and polarization of charges at the electrochemical interface that can only be achieved by computationally expensive quantum chemistry methods [11–13].

As explained by Trasatti [8, 14–16], the absolute electrode potential is related to the work function of the electrode in the presence of an electrolyte layer. In particular, the potential of zero charge (pzc) is given by the work function of the electrode covered by a pure and ion-free water film and can be measured experimentally. It is important to note that charge polarization at the interface between electrode and electrolyte contributes to the change of the work function and thus of the electrode potential.

However, within electronic structure theory, there is no practical implementation to treat the electrode potential as a parameter in a so-called constant potential method within a grand canonical ensemble. Rather, quantum chemistry programs typically optimize a solution with a constraint with respect to the number of electrons leading to constant electron methods within a micro-canonical ensemble. Another obstacle is the liquid nature of electrolyte requiring numerically demanding statistical averages since many nearly degenerate configurations have to be thermodynamically sampled to address the entropic contributions properly. In a quantum chemical approach, these averages have to be performed on the basis of ab initio molecular dynamics (AIMD) simulations, which had been considered to be computationally too demanding for the description of complex electrochemical interfaces [17–19].

When at the electrochemical interface positive or negative ions are present, then the electric double layer and the electrode potential will be accordingly changed from the potential of zero charge. As demonstrated in various experimental and theoretical studies [20–26], one of the simplest ways to introduce ions into the water film is to control the pH of the aqueous electrolyte by adding or subtracting H atoms which will lead to the spontaneous formations of hydronium or hydroxyl ions. When the ion distribution in the electrolyte is in thermodynamic equilibrium, then the averaged charge polarization at the electrochemical interface will correspond to the electric double layer at a specific electrode potential.

As the computer power increases, electrochemical systems are becoming accessible to first principles simulations [25, 27–29]. For example, AIMD simulations have already been performed yielding values of the pzc close to experimental values [28, 29]. Here we extend this approach by demonstrating that adequately prepared AIMD trajectories can produce a proper polarization distribution within the electric double layer yielding a corresponding electrode potential. When the fluctuations at thermal equilibrium are not too large, then the statistical properties can be reliably sampled by relatively short trajectories.

Within this approach, the electrode potential is no control parameter of the simulations, but established by appropriate atomic configurations at the electrode-electrolyte interface. Then, the polarization distribution

* sung.sakong@uni-ulm.de
† axel.gross@uni-ulm.de

in thermodynamic equilibrium provides basic information about the electrified electrochemical interface without explicit consideration of a counter electrode [30, 31]. Our approach is similar in the spirit to the one developed by Rossmeisl and co-workers [11, 32] resulting in the concept of the generalized computational hydrogen electrode [24, 33], but is based on a larger sampling set in order to correct for the finite size of the surface unit cell in the simulations.

In this study, we will particularly consider electrochemical interfaces between Pt(111) and a water film which additionally contains ions such as hydronium and hydroxyl ions [34–41]. By performing AIMD simulations we will elucidate the structure of the electric double layer and derive the corresponding electrode potential.

II. COMPUTATIONAL DETAILS

The AIMD simulations have been performed using the periodic density functional theory package VASP [42]. The wave functions were expanded up to a cutoff energy of 400 eV using a plane wave basis set and the electronic cores are described by the projector augmented wave (PAW) method [43]. Exchange-correlation energies are evaluated within the generalized gradient approximation as suggested by Hammer and Nørskov, known as a revised version of the Perdew-Burke-Ernzerhof (RPBE) functional [44]. Dispersion effects have been considered within the semi-empirical D3 dispersion correction scheme of Grimme using the zero damping function [45–47]. The RPBE-D3 approach correctly predicts properties of liquid water [28, 48, 49]. In addition, it reliably describes the interaction of organic molecules [50, 51] and water [28, 48, 49] with metal surfaces. The cutoff radius for the pair interactions of D3 correction has been chosen to be 10 Å. However, the screening of the van der Waals interactions in bulk metals is not correctly described in dispersion correction schemes [48, 51–53]. Therefore we exclude the dispersion correction for all metal atoms below the first layer. The energies have been determined within a 6×6 surface super cell employing at the Gamma k-point of the first Brillouin zone. The energies of each ionic step satisfy the convergence criteria of 10^{-6} eV.

The thermodynamic properties of liquid water have been derived from ab initio molecular dynamics (AIMD) simulations with a time step of 1 fs. Note that the hydrogen and not the deuterium mass was used in the MD simulations. The density of liquid water at 298 K ($1\mathrm{g/cm^3}$) is emulated by 96 water molecules in a cubic cell of 14.2 $\mathrm{Å}^3$. The equilibrium state of the canonical NVT ensemble at 298 K has been calculated by solving the Langevin equation with a friction coefficient of $\gamma = 5\,\mathrm{ps}^{-1}$. The system has been thermalized for 10 ps, and the statistical sampling has been performed during the subsequent 40 ps run.

The water metal interface is modeled by 144 water molecules within a 6×6 unit cell corresponding to six layers of water on a five-layer Pt(111) slab. The integration over the first Brillouin zone is replaced by a summation over the Gamma k-point which is adequate due to the large size of the unit cell. For bulk Pt, a lattice constant of 3.99 Å is obtained using a fine k-point grid of $21\times21\times21$ and the RPBE functional. The top three layers of the Pt slab are fully relaxed, while the bottom two layers are fixed at their bulk positions. The water film has a thickness of about 20 Å separated by 15 Å of vacuum from the next metal slab. The AIMD simulations for the Pt(111)-water interface have been performed using the same setup as for the bulk liquid water simulations. In addition, we have performed an extra 30 ps AIMD run with less tight energy convergence criteria to thermalize the water structure.

The characteristics of the electric double layer is mainly determined by the polarization distribution. Technically, there is a certain ambiguity to assign partial charges to specific atoms. Using localized wave function based based methods, a charge polarization can be estimated by monitoring the Mullikan charge of each atom. Within plane-wave based periodic density functional theory (DFT) calculations, a charge partitioning scheme is necessary to define the net atomics charge (NAC) of each atom. Then, the polarization of each atom can be monitored as a change of the NAC from a reference value. There are several feasible techniques available such as the density derived electrostatic and chemical (DDEC) [54–57] or the Bader charge [58–62] methods. Here, we have used the DDEC method which determines the NAC from an equivalent atomic charge distribution that reproduces the DFT electrostatic potential. The polarization distribution can then be estimated by averaging the NAC change over AIMD trajectories.

Polarization distributions are evaluated by the change of net atomic charge (NAC) of each atom using DDEC method [54–57]. The reference NAC e_{i0} of H and O species is determined by a molecular dynamics simulation of bulk liquid water using 96 water molecules in a box at 298 K. The NAC has been sampled every 1 ps and averaged up to 80 ps. The e_{i0} of the layers of the Pt electrode is evaluated using a Pt(111) slab in vacuum. In Table II, the reference NAC of H, O, and Pt species are listed. The NAC of H and O in liquid water reproduces the experimental findings. The NAC with the Pt slab shows a Friedel oscillation along the surface normal direction.

III. CONSTRUCTION OF ELECTROCHEMICAL INTERFACES

We will first address the Pt(111)/water interface at the potential of zero charge. The electrochemical interface between a Pt(111) electrode and an aqueous electrolyte at pzc is prepared as suggested by Trassati [8, 14–16], i.e., it is formed by an ion free water film on a Pt electrode. Here we modeled this particular system by 144 water

molecules on a Pt(111) slab with a 6×6 surface unit cell which is separated from its periodic images by a vacuum layer of 1.5 nm. The water film is about 2 nm thick which corresponds to six water bilayers, and the Pt slab consists of five atom layers with an optimized fcc lattice parameter of $a = 3.99$ Å as shown in Fig. 1a. The liquid configuration of the water film is prepared by a 30 ps long thermalization period at 298 K employing low accuracy calculations followed by a further 10 ps thermalization at high accuracy. Note that with respect to our previous study [28], the size of the surface unit cell is enlarged by a factor of four.

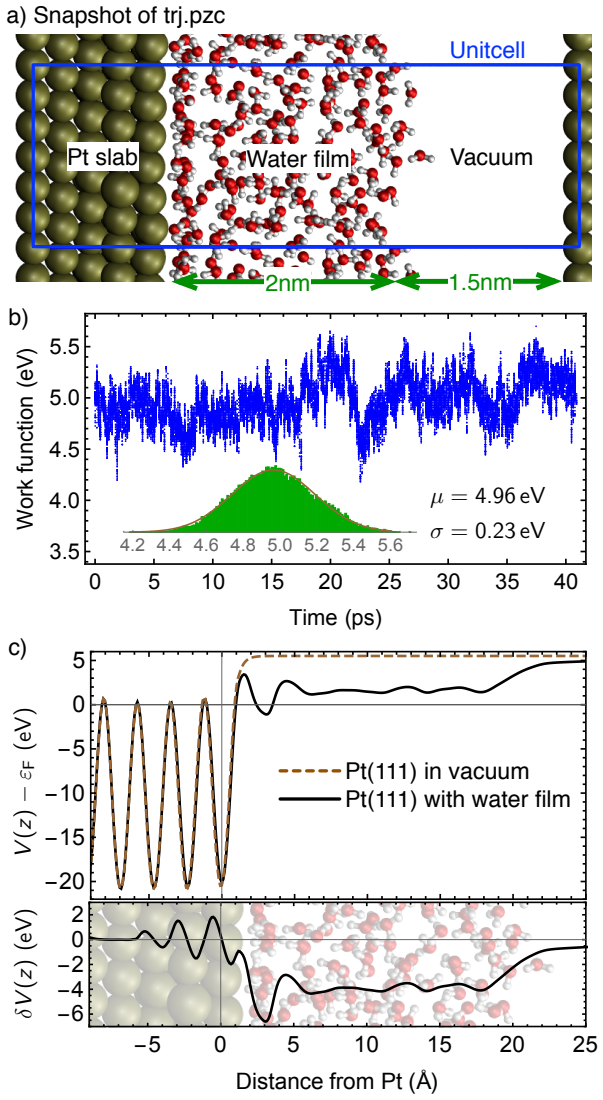

FIG. 1. a) A snapshot and b) time evolution of the work function along the trajectory to determine the potential of zero charge (trj.pzc) equilibrated at 298 K. c) Electrostatic potential $V(z)$ of Pt(111) in vacuum (dashed green line) and the averaged potential of the Pt(111) electrode with an ion free water film (black line). The change caused by the water film $\delta V(z)$ (red line) is illustrated in the lower panel.

A canonical ensemble at 298 K is then sampled during 40 ps by solving the generalized Langevin equation with a time step of 1 fs and a friction coefficient of $\gamma = 5/\text{ps}$. The sampled temperatures satisfy a Gaussian distribution $\sim \exp[-(T-\mu)/2\sigma^2]$ with a mean temperature of $\mu = 299$ K and a variation of $\sigma = 10$ K. We note that the variation is smaller than in our previous simulations [28] due to the four times larger supercell. In addition to the temperature, properties such as the potential energy and work function follow Gaussian distributions indicating an appropriate sampling within a canonical ensemble. The sampled work function of the ion-free water film is 4.96 eV with $\sigma = 0.23$ eV, as shown in Fig. 1b. The result is in good agreement with the experimental measurement [14] as well as the previous simulations [28].

It is important to realize that in our statistical ensemble we include water structures that are characterized by work functions that do not correspond to the pzc. However, in the simulations we employ a surface unit cell of finite size which is in fact still rather small. The electrode potential is a macroscopic property, and the appropriate ensemble will contain electrode/electrolyte structures that locally lead to a range of work functions. Thus by considering structures with different work functions we effectively sample over these local structures. It is only critical that the distribution in the work function is symmetric with respect to the mean value which is ensured by the Gaussian shape indicated in Fig. 1b.

In Fig. 1c, the averaged electrostatic potential of the ion-free water film (solid black line) and the electrostatic potential of Pt(111) in vacuum (dashed green line) are plotted with the Fermi levels being aligned. We note that the potential in the water film in the range between 5 and 18 Å away from the Pt(111) electrode is rather flat and smooth. This indicates that the film aquires properties of bulk liquid water which at the same time demonstrates that a water film of 2 nm thickness is sufficient to reproduce the properties of the aqueous electrolyte.

The electrostatic potential is plotted with respect to the electron whereas in electrochemistry typically potentials are plotted with respect to a positive probe charge. Hence to compare the electrostatic potential plotted in Fig. 1c with typical graphs derived from continuum theory [4–6], its sign needs to be flipped. There is no monotonic behavior of the potential as predicted by the continuum theories, but rather an oscillatory behavior. The layered structure of water at Pt(111) even at room temperature is still visible. Furthermore, from the range of the decay of the electrostatic potential to the mean value in the bulk liquid, a thickness of the electrical double layer at pzc of below 1 nm can be derived. However, it is also obvious that it is not so easy to assign the exact location of the electric double layer given the broad continuous variation of the electrostatic potential.

In the vacuum region, the electrostatic potential above the water film stays below the potential above the uncovered Pt(111) electrode. This difference corresponds to the decrease of the work function of Pt(111) from 5.01 eV

to 4.96 eV due to the presence of the water film. At the electrochemical interface between the electrode and the electrolyte, we see a strong dip of the potential at the solvating water layer compared to the bulk liquid water. This is indicative of a positive charge polarization. In addition, Friedel oscillations occur within the Pt(111) slab to screen this strong charge polarization. We stress that the charge polarization is a microscopic phenomena and can not be explained by any proposed electrostatic models based on a point charge scheme. We will discuss the details of the polarization at the interface using the charge partitioning method in Section V.

The pH of the aqueous electrolyte is changed by adding or removing one H atom (a proton and an electron) in the water film. The additional H atom then spontaneously forms a hydronium or a Zundel complex while the electron is transferred to the Fermi level in the metal [22, 24, 25]. In contrast, the H vacancy leads to the formation of a hydroxyl ion with an electron taken from the Fermi level. In the simulations, one additional proton in 144 water molecules corresponds to a pH of 0.4, whereas one hydroxyl ion corresponds to a pH of 13.6 (pOH = 0.4) based on the self-ionization of aqueous water molecule. Upon adding and removing an H atom, we have further thermalized the liquid water configuration for 10 ps and then sampled over 40 ps.

A solvated proton in a water film is a highly dynamic entity. The proton is transferred from one water molecule to another easily and can be simultaneously shared by more than one water molecule. The presence of the solvated proton influences not only the nearest water molecules, but also the water molecules located further away. In order to characterize the dynamics of the solvated proton, we monitor the neighboring H atoms of each oxygen atom. The H atoms within 1.43 Å (corresponding to 1.2 times the sum of the Wigner-Seitz radii of O and H) are considered to belong to an oxygen atom. When an oxygen atom has three neighboring H atoms, then the oxygen is assigned as a proton active site. An isolated proton active molecule represents a hydronium configuration. When two proton active molecules sharing a hydrogen atom co-exist, then the configuration is regarded as a Zundel complex.

When we apply the analysis regarding the proton activity to the trajectory of the ion-free water film (trj.pzc), we notice a proton activity in the solvating water layer up to 5 Å away from the topmost Pt layer (see black line in Fig. 2a) in spite of the fact that no explicit ions were introduced into the water film. The hydronium configuration emerges when two water molecules approach each other closely enough and one of the H atoms is simultaneously shared by the two water molecules. The population probability is about 10 % per time step. Further away from the electrode, in the bulk liquid-like region no proton active molecules are observed. Obviously the electrode drives this formation. As a result, the solvating water layer becomes acidic although the water film is in principle ion-free. Actually, the proton activity in

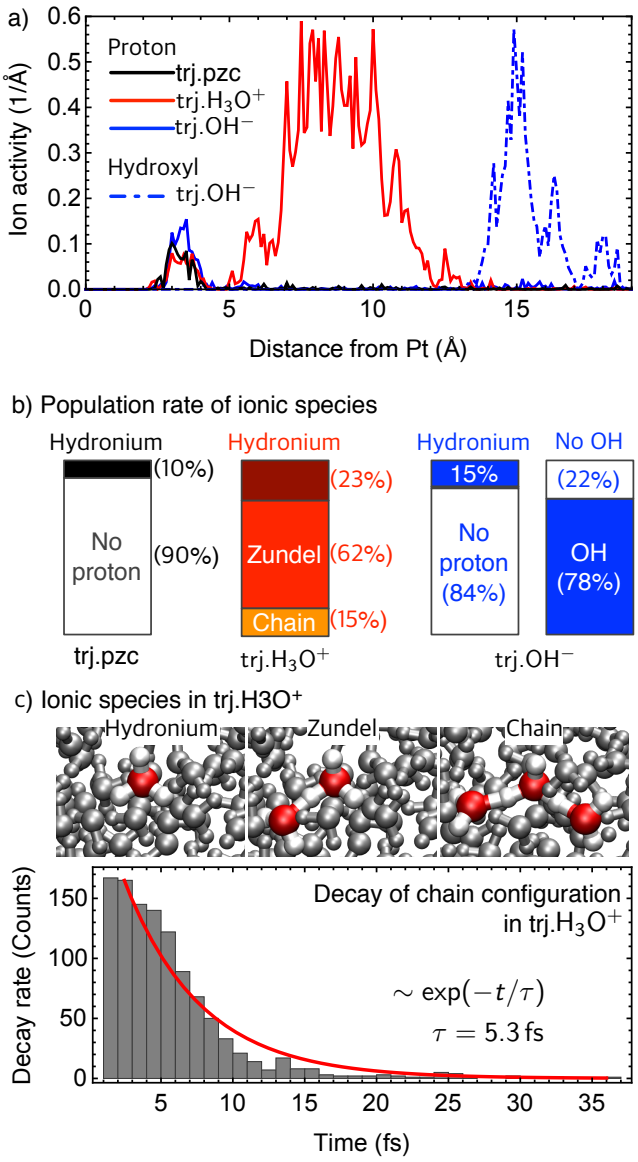

FIG. 2. a) Distribution of ion activity in water film without any additional ion (trj.pzc, black line), with one H_3O^+ formation (trj.H_3O^+, red line), and with one OH^- formation (trj.OH^-, blue and green lines). b) Population probability of proton and hydroxyl in the water film. c) Snapshots of hydronium, Zundel and instant chain configurations in trj.H_3O^+. Decay rate of chain configuration.

the solvating water layer contributes to the dip of the electrostatic potential at the interface shown in Fig. 1c.

When adding one H atom into the water film (trj.H_3O^+), we note that in every time step along the simulation time there is at least one oxygen atom within the simulation box that has three neighboring H atoms. The population density in Fig. 2a (red line) shows that the additional H atom leads to a strong proton activity in the range from 5 to 14 Å above the electrode. The most abundant proton active molecule is the Zundel ion (62 %

population). The population of hydronium corresponds to 23 % which is increased by 13 % compared to the ion-free water. Furthermore, water chains are formed that are illustrated in Fig. 2c. Their population probability is 15 %, however, they quickly decay to Zundel ions within about 5 fs, as also shown in Fig. 2c.

Figure 2a shows the population of hydroxyl ions in the water film (trj.OH^-, blue dashed line). Interestingly enough, upon removing one H atom, the OH^- species are less mobile than the protons, and they are mainly located at a distance between 13 and 19 Å from the electrode (blue dashed line in Fig. 2a). Solvated hydroxyl ions cause a strong rearrangement of the surrounding water molecules. To be specific, the surrounding water molecules build up a strong solvation shell around and the OH^- species form instant $OH^-(H_2O)_n$ complexes ($n = 1, 2$). As a result, as shown in Fig. 2c, there is no hydroxyl configuration, i.e., a hydrogen atom close to the OH group, in 22 % of the steps.

We still find proton activity in the solvating water layer (see full blue and red lines in Fig. 2a) even if one hydrogen atom has been added or removed. The population density becomes slightly smaller than the ion-free water film in the presence of a positively charged ion in the double layer, whereas the density becomes slightly larger in the presence of a negatively charged ion. Interestingly enough, the proton activity close to the electrode is rather similar in all considered three cases. Obviously the presence of ions, both proton or OH^-, in the water film farther away from the electrode hardly influence the acidic behavior close to the electrode.

The ion species created in the water film mainly exist above the solvating water layer. The distributions of the positively and negatively charged ion species are clearly separated. The positive ions are available close to the interface (in the range of 5 to 14 Å), whereas the negative ions exist farther away from the interface (in the range of 13 to 19 Å). The presence of ions in the water film modifies the work function with respect to the ion-free water case as demonstrated in Table I. The presence of a proton decreases the work function by 0.11 eV, whereas the hydroxyl ion increases it by 0.09 eV.

Frumkin and Petrii [20] have shown a linear behavior of the pH dependent electrode potential experimentally, in acidic condition a potential change of 13 mV/pH and in alkalic condition of 11 mV/pH. These numbers are in good agreement with the work function change of 17 mV/pH in acidic condition and 14 mV/pH in alkalic condition, respectively. This yields credibility to our simulations of electrochemical interfaces and the derived absolute electrode potentials.

TABLE I. Work function Φ averaged along the trajectories of a water film consisting of 144 H_2O molecules on a (6×6)Pt(111) electrode plus different numbers of hydogen atoms given by ΔH. The trajectories are sampled for 40 ps at 298 K. The electrode potential U is determined with respect to the standard hydrogen electrode of 4.44 V. The net atomic charge of the Pt slab (NAC_{Pt}) corresponds to the sum over the changes in the charge polarizations over the Pt atoms with respect to bulk Pt.

Trajectory	ΔH	Φ (eV)	pH	U (V)	NAC_{Pt} (e)
trj.pzc	0	4.96 ± 0.23	7.0	0.52	−1.25
trj.H_3O^+	+1	4.85 ± 0.25	0.4	0.41	−1.56
trj.OH^-	−1	5.05 ± 0.19	13.6	0.61	−0.93
trj.H_{ads}	+1	4.92 ± 0.20	7.0	0.48	−1.27
trj.OH_{ads}	−1	4.93 ± 0.21	7.0	0.49	−1.08
trj.$36H_{ads}$	+36	4.91 ± 0.20	0.1	0.47	−1.03
trj.$2H_3O^+$	+2	4.86 ± 0.20	0.1	0.42	−1.84

IV. ADSORBATES ON THE Pt ELECTRODE

Here, we consider the properties of H and OH adsorbed on the Pt electrode. An H atom deposited on the electrode (underpotential deposition of hydrogen [63], see trj.H_{ads}) remains adsorbed on the electrode along the whole trajectory of 40 ps, i.e. we did not observe any proton transfer into the water layer. Such events can only be observed within AIMD simulations when a weakly adsorbed hydrogen atom is added to a Pt(111) electrode already covered by one monolayer of hydrogen [64]. In contrast, when an hydroxyl is adsorbed on the electrode, then water structures corresponding to the hydroxyl configuration are created in the solvating water layer with a probability of 71 % which is slightly lower than the probability in the water film of 78 %. This in fact means that the adsorbed hydroxyl is more strongly interacting with the surrounding water molecules than the hydroxyl ion in bulk water. As an example, snapshots (ii), (iii), and (v) in Fig. 3a illustrate the formation of the strongly interacting hydroxyl-water complexes on the Pt(111) surface.

According to our simulations, H diffusion on Pt(111) proceeds via explicit hops of the adsorbed H atom whereas the OH diffusion is mediated through proton transfer from a solvating water molecule to the hydroxyl, similar to the Grotthuß mechanism of proton diffusion in bulk water [36]. As a result, hydroxyl is created at a neighboring water site as demonstrated in Fig. 3a. In the trajectory of trj.OH_{ads}, we note that up to three O sites are involved in the OH propagation. Each oxygen atom is localized at a specific Pt site. In total we observed 78 such OH hopping events during the whole simulation time of 40 ps.

In Fig. 3b, the proton activity in the presence of the H and OH adsorbate is compared to the ion activity of the pure water film (trj.pzc). An example configuration of the proton activity is displayed in the inset window. In all considered cases, the proton activity remains within the solvating water layer. The averaged work functions along trj.H_{ads} and trj.OH_{ads} are 4.92 and 4.93 eV (see Table I). The relatively small change in the work function from the ion-free water film is consistent with the

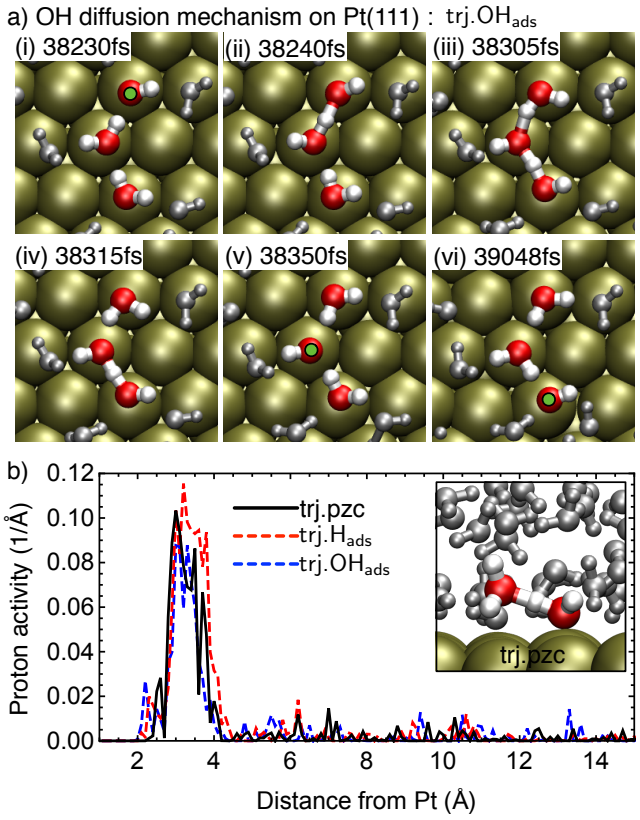

FIG. 3. a) Snapshots of OH diffusion mechanism on Pt(111) electrode along trj.OH_{ads}. The water molecules associated with the Grotthuß mechanism of proton transfer are highlighted in color. b) Proton population along trj.pzc, trj.H_{ads}, and trj.OH_{ads}. In the inset, a snapshot of proton activity in the solvating layer of trj.pzc is demonstrated.

similar proton activity in the water film to the trj.pzc. Thus, the proton activity in the solvating water layer is mainly caused by the interaction between the electrode and the solvating water molecules, and the presence of adsorbates with a low concentration hardly affects the electrical double layer.

Next, we consider a fully hydrogen covered electrode (trj.36H_{ads}) to simulate the electrochemical interface at low electrode potentials [19, 51, 65]. Initially, all Pt sites are saturated by H atoms (in total 36 H atoms per unit cell) and thermalized for 10 ps. During thermalization, two H atoms spontaneously desorb from the surface and form proton configurations in the water film. The corresponding pH of the electrolyte is then changed to 0.1, corresponding to strongly acidic conditions. This configuration is stable along the whole 40 ps of the AIMD trajectory.

Interestingly, we also find a change of the structure of the electrochemical interface. In Fig. 4a, the distribution of water molecules is represented by the distribution of corresponding oxygen atoms. When we consider the ion-free water film (see upper panel), the solvating water layer is closely packed and the density is close to the ice-like bilayer [28]. However, the presence of the hydrogen monolayer lifts the whole water film by around 1 Å from the Pt electrode as already observed in our group [66]. The adsorbed hydrogen layer weakens the Pt-water interactions and leads to the larger distance of the solvating water layer from the surface. Due to the weaker interaction, the solvating water layer becomes broader, the deconvolution in the lower panel of Fig. 4a indicates that the layer extends up to 8 Å from the Pt surface. Thus also the overlap between the solvating water layer and the bulk liquid water becomes larger. Furthermore, the solvating water layer is split into two Gaussian functions (see lower panel). The peak at 3.8 Å originates from the water molecules directly interacting with two Pt regions that are covered by an adsorbed hydrogen atom, whereas the peak at 4.7 Å corresponds to the remaining lifted solvating water layer.

These structural changes are illustrated in Fig. 4b where snapshots of trj.36H_{ads} and trj.pzc are displayed. Note that there is a spatial separation between the solvating water layer and the bulk-like water in trj.pzc, highlighted by the additional background color, whhereas for trj.36H_{ads} no clear separation can be observed. This confirms that the structure of the electrochemical interface is influenced by the presence of adsorbates. The work function along trj.36H_{ads} is 4.91 V which is lowered by only 0.05 V compared to trj.pzc, in spite of the strong proton activity in the water film. This indicates that the polarization due to the proton activity in the water film is largely compensated by the rearranged water structure.

In order to identify the influence of the acidic electrolyte, we have also performed a simulation with two protons in the water film without any hydrogen adsorbates on Pt(111) (see middle panel in Fig. 4a, trj.2H_3O^+). The comparison with the upper panel indicates that the presence of the two protons in the film hardly modifies the water distribution (see middle pannel in Fig. 4a). The deconvolution of the Gaussian functions (dashed lines) shows that the solvating layer stays intact at 3.2 Å above the Pt electrode. This means that the modified structure of the solvating layer on hydrogen-covered Pt(111) with respect to uncovered Pt(111) is not caused by the presence of the two protons in the water film.

The stability of the hydrogen layer has been tested by filling the two empty hydrogen adsorption sites of trj.36H_{ads} with two additional H atoms (trj.38H_{ads}). The Pt(111) electrode in fact remained fully hydrogen-covered in the acidic electrolyte along the AIMD run. However, the free energy difference between trj.36H_{ads} and trj.38H_{ads} is 0.2 eV smaller than the energy of H_2 molecule. This means that the system would gain energy if two adsorbed hydrogen atoms desorb associatively into the gas phase. Thus, the energetics indicate that the fully hydrogen-covered Pt electrode is less stable than the H layer with a lower coverage. The spontaneous desorption of H atoms is consistent with the experimental findings of a hydrogen saturation coverage on Pt(111) of less than

one [67].

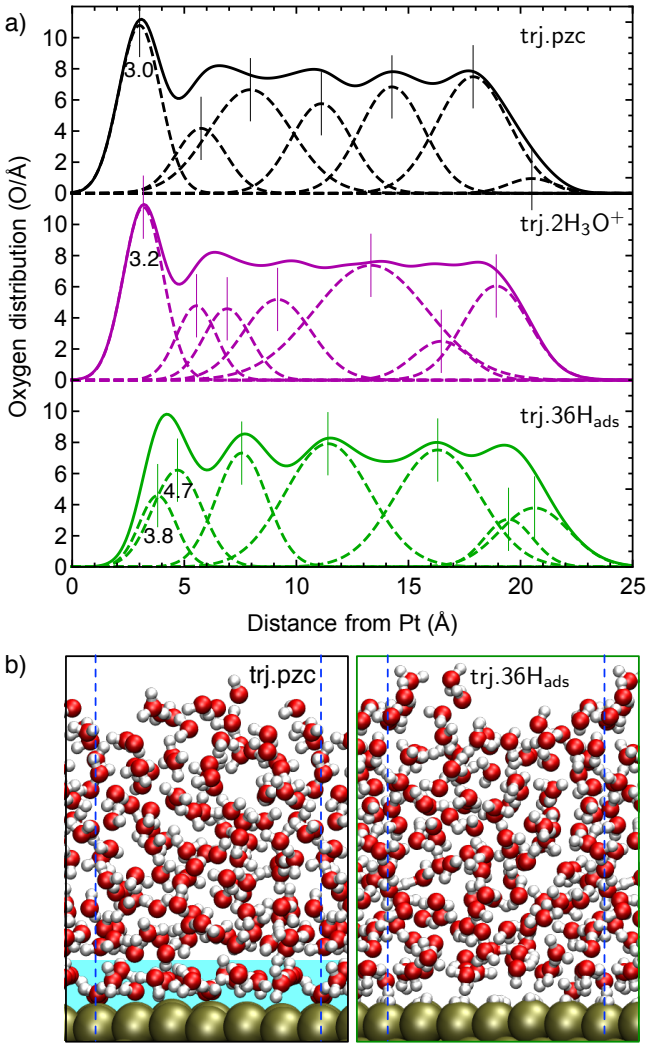

FIG. 4. a) Distribution of oxygen atom in the water film of the trj.pzc (black line, upper panel), trj.2H_3O^+ (blue line, middle panel), and trj.36H_{ads} (red line, lower panel). The deconvolution of oxygen distributions in terms of Gaussian functions is depicted as green lines. b) Snapshots of trj.pzc and trj.36H_{ads}.

V. CHARGE ANALYSIS

The electrostatics at the electrochemical interface depends mainly on the charge polarization. As a simplistic approach, we will derive the charge polarization from the change in the net atomic charge (NAC). However, since there is no explicit description of localized orbitals within plane wave based methods, a charge partition scheme is necessary to attribute DFT charge densities to a particular atom [54–57]. From the NAC $e_i(z,t)$ of species i sampled at time step t, the polarization is determined according to

$$P(z) = \left\langle \sum_i e_i(z,t) - e_{i0} \right\rangle_t \qquad (1)$$

with the reference NAC (e_{i0}) as given in Table II. A negative value of $P(z)$ represents an electron surplus, while a positive value indicates an electron depletion.

As listed in Table II, the reference species correspond to a Pt electrode in vacuum and bulk liquid water. The deviation from the references effectively represents the polarization of each atom. The atomic polarization is smeared in the form of Gaussian distribution with a width of 0.5 Å and laterally integrated. The polarization distribution is determined every 500 fs, i.e., the polarization is averaged over 80 charge density snap shots.

TABLE II. Reference of the net atomic charge e_{i0} of H, O, and Pt species, with the NAC of the corresponding atomic species taken to be zero.

	Water		Pt(111)				
Species	H	O	Pt_{1L}	Pt_{2L}	Pt_{3L}	Pt_{4L}	Pt_{5L}
e_{i0}	0.38	−0.76	−0.030	0.034	−0.005	0.032	−0.030

Figure 5a shows the polarization distribution of trj.pzc. Interestingly, the formation of an interface dipole ($\bar{\mu}_{\text{int}}$) which is induced by a partial charge transfer from the solvating water layer to the electrode is clearly visible. Such a partial charge transfer has also been observed for an oxide/liquid water interface [10] and Pt/water interface [29]. According to Table I, the NAC of the Pt slab corresponds to 1.25 electrons, thus a little bit more than one electron is transferred from the solvating water layer to the Pt(111) slab within a (6×6) supercell. The negatively charged electrode lowers the work function compared to the Pt electrode in vacuum (see Fig. 1c) and reproduces the absolute electrode potential of the ion-free water film correctly. As a result, the solvating water layer becomes more positively charged than bulk liquid water and exhibits proton activity despite the absence of explicit ions in the water film as shown in Fig. 2a. The charge polarization is purely dipole-like and mainly localized in the first Pt layer and the solvating water layer. The integrated polarization distribution vanishes at a large distance from the interface as shown in Fig. 6a.

As shown by Trassati [8, 14], the electrode potential can be derived from the work function of a metal electrode in contact with an electrolyte. Thus the electrode potential is influenced by any preferential re-orientation of the solvating molecules at the interface. Recent AIMD based studies [19, 29, 68] show that there is no preferential orientation of water molecules in the solvating layer on Pt(111). Thus, the dipole contribution of the solvating water layer to the electrode potential is rather small due to cancellation effects upon the statistical averaging. The polarization at the interface is in fact mainly

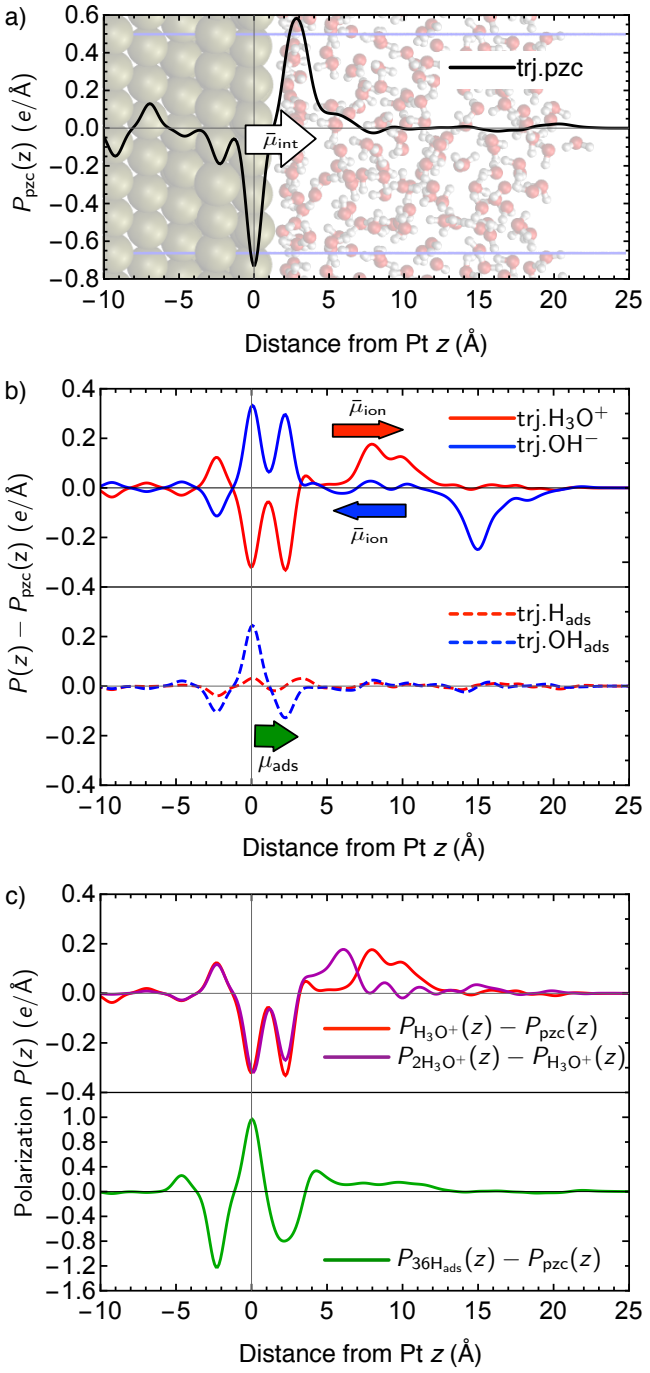

FIG. 5. a) Polarization distribution $P_{pzc}(z)$ of the trj.pzc. b) Polarization change compared to trj.pzc ($\delta P(z) = P(z) - P_{pzc}(z)$) in trj.$H_3O^+$, trj.$OH^-$, trj.$H_{ads}$, and trj.$OH_{ads}$. c) Polarization change of trj.$2H_3O^+$ and trj.$36H_{ads}$.

caused by the partial charge transfer from the solvating layer to electrode (see Fig. 5a). As a result, the interface dipole created by the partial charge transfer dominates the work function change. This atomistic analysis of the factors determining the polarization at the interface allows to unambiguously specify the different contributions to the interface dipole and thus goes beyond empirical assumptions.

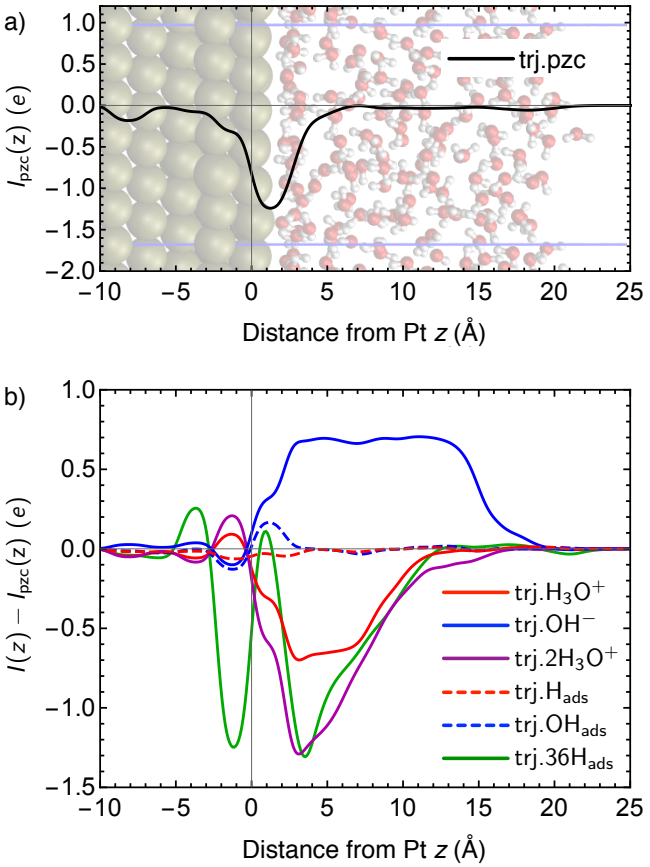

FIG. 6. a) Integral polarization $I_{pzc}(z) = \int^z P(z')dz'$ of the trj.pzc. b) Change of the integral poralization compared to the trj.pzc ($\delta I(z) = I(z) - I_{pzc}(z)$) in the trj.$H_3O^+$, trj.$OH^-$, trj.$H_{ads}$, and trj.$OH_{ads}$.

When ions are present in the water film, also the bulk liquid water becomes polarized. As depicted in the upper panel of Fig. 5b, the presence of a proton in the water film polarizes the water film positively compared to the ion-free electrolyte, while OH^- polarizes the film negatively. These polarizations in the water film are partially compensated by an opposite polarization at the Pt-water interface. These additional polarizations upon introducing ions into the water film alters the work function compared to the ion-free case (see Table I).

The addition or removal of an H atom corresponds to a change by one electron and a proton. After addition or removal of an H atom, the charges of the H and O atoms in liquid water are quickly equilibrated towards the reference values in Table II. This is due to the fact that the additional H atom or the remaining OH group, respectively, quickly become part of the dynamic hydrogen-bonded water network so that there electronic properties become strongly coupled to the other water molecules.

Along the trj.H_3O^+ trajectory, the formation of one

hydronium ion leads to an increased electron population in the Pt electrode by $0.3\,e$ compared to the trajectory trj.pzc (see Table I). As shown in the integral polarization in Fig. 6b, the negative polarization is increased to $-0.7\,e$ in the solvating water layer and screened by the positive ion in the water film. After the maximum integral polarization, we note a plateau up to 7 Å which indicates that the negative polarization at the interface is well separated from the positive polarization in the water film. Thus, this shows an additional dipole formation by the ion population in the water film $\bar{\mu}_{\mathrm{ion}}$ along the interface normal direction on top of the interface dipole $\bar{\mu}_{\mathrm{int}}$. However, according to the electron count not a full electron is transferred to the electrode leaving a proton in the water film. This indicates that the electron distribution is not localized within the electrode and the solvating water layer, but extended into the water film. As a result, the proton polarization is partly screened by the extended electron distribution. Such an extended electron distribution can only be obtained in an explicit quantum chemical description of the electrolyte and cannot be simulated by a charged metal slab in vacuum with matching a boundary condition [69, 70]. This demonstrates that it is crucial to explicitly determine a realistic polarization distribution at electrode-electrolyte interfaces.

In contrast to hydronium formation, OH^- formation in the water film (trj.OH^-) leads to a depletion of the electron density in the Pt electrode and the solvating water layer (see blue solid line in Fig. 5b). The positive polarization amounts to about $+0.7\,e$ as shown in the integral polarization in Fig. 6b. The OH^- ion induced dipole $\bar{\mu}_{\mathrm{ion}}$ is oppositely oriented with respect to the hydronium induced dipole which is consistent with the work function increase or decrease, respectively, listed in Table I.

When an H atom is deposited on the Pt surface at a coverage of 1/36 (trj.H_{ads}) O^+, the NAC of H becomes close to zero. This is also reflected in the negligible polarization change shown in the lower panel of Fig. 5b. Thus, the influence of a low coverage deposition of H on the polarization of the electrochemical interface is rather small and only leads to a minor change in the work function with respect to the pzc.

With respect to the formation of OH in the solvating water layer (trj.OH_{ads}), for the O atom we take the same NAC reference in the hydroxyl molecule as for trj.OH^-. As shown in Table I, there is only a small amount of electron transfer from the Pt electrode to the hydroxyl molecule, indicated by the small difference in the NAC_{Pt} values for trj.pzc and trj.OH_{ads}. The partial charge transfer leads to a further change on the charge polarization at the interface. As Fig. 5 shows, the ion induced polarization is symmetric along the interface normal with respect to the position of the Pt surface atoms. Thus, the net contribution to the ion-induced dipole $\bar{\mu}_{\mathrm{ion}}$ is small.

In vacuum, OH adsorption on Pt(111) at the same coverage leads to a work function change of 0.05 V [71, 72]. According to Table I, the change is reduced to 0.03 V in the presence of the solvating water molecules. This indicates that the adsorbate induced dipole contribution becomes screened by the liquid water. Consequently, we assign the rest of the dipole formation to an adsorbate induced dipole $\bar{\mu}_{\mathrm{ads}}$. We note that the three dipole contributions $\bar{\mu}_{\mathrm{int}}$, $\bar{\mu}_{\mathrm{ion}}$, and $\bar{\mu}_{\mathrm{ads}}$ at the electrochemical interfaces are additive. Then, in general, the work function of the electrochemical interfaces can be expressed by

$$\Phi = \varepsilon_{\mathrm{F}} + \mu_{\mathrm{surf}} + \bar{\mu}_{\mathrm{int}} + \bar{\mu}_{\mathrm{ion}} + \bar{\mu}_{\mathrm{ads}} \qquad (2)$$

with the bulk Fermi level ε_{F} of the electrode and the surface dipole at the solid/vacuum interface μ_{surf} [73].

For the fully hydrogen covered surface trj.$36H_{\mathrm{as}}$, a decrease of the partial charge transfer from the solvating water layer to the Pt electrode due to the increased distance between Pt and water film by the adsorbed H layer is observed (see Tab. I). As mentioned above, the contribution of a isolated adsorbed H atom to the polarization distribution at the interface is negligible, but the weakened solid/liquid interaction at the interface makes the interface dipole $\bar{\mu}_{\mathrm{int}}$ smaller than for the trj.pzc. However, the formation of two proton ions in the water film leads to the formation of $\bar{\mu}_{\mathrm{ion}}$ which compensates the decrease of $\bar{\mu}_{\mathrm{int}}$. As a result, the polarization change of trj.$36H_{\mathrm{as}}$ is rather symmetric with respect to the uppermost surface layer as shown in Fig.5c, and the work function is only changed to 4.91 eV which is still close to the pzc of 4.96 eV.

Thus, the formation of interface dipoles also depends on the strength of the solid/liquid interaction [30]. High coverage adsorbates on electrode can modify the interface dipole and consequently also the electrode potential [74]. This also indicates that the partial charge transfer on noble metal electrodes which interact weakly with solvating water molecules should be small. Consequently, other contributions to the work function change become critical.

We note that the three different configurations of the electric double layer (trj.H_{ads}, trj.OH_{ads} and trj.$36H_{\mathrm{ads}}$) all lead to a rather similar work function of about 4.92 V as shown in Table I. Thus, different configurations can result in the same electrode potential. Especially, a polarization distribution that is symmetric with respect to the uppermost surface layer hardly causes any change in the work function as the contributions from different locations cancel each other.

VI. COMPUTATIONAL HYDROGEN ELECTRODE AND FREE ENERGIES

Here we will analyze the stability of the system along the trajectory trj.H_3O^+ using a grand canonical approach. The reference system will be the trajectory corresponding to the pzc described by an ion free water film on the Pt electrode. The addition and removal of an H atom can be treated by the computational hydrogen electrode (CHE) approach as suggested by Nørskov [32, 75, 76].

The electrochemical potential of a proton in aqueous solution can be described using

$$\tilde{\mu}_{\mathrm{H^+(aq)}} + \tilde{\mu}_{e^-} = \frac{1}{2}\mu_{\mathrm{H_2(g)}} - eU_{\mathrm{SHE}} - k_{\mathrm{B}}T\ln(10)\mathrm{pH}, \quad (3)$$

where one has used the fact that at standard conditions defining the standard hydrogen electrode potential U_{SHE} the solvated proton is in equilibrium with the H_2 molecule in the gas phase. This approach avoids the explicit evaluation of solvation energies of ionic species [19, 77–80].

Since trj.H_3O^+ is created by adding one H atom into trj.pzc, the free energy of trj.H_3O^+ should correspond to the free energy obtained by averaging along trj.pzc plus the energy of a solvated hydrogen given by the expression according to the computational hydrogen electrode at an absolute potential of 4.85 V (see Table I),

$$\langle E_{\mathrm{trj.H_3O^+}}\rangle = \langle E_{\mathrm{trj.pzc}}\rangle + \tilde{\mu}_{\mathrm{H^+(aq)}} + \tilde{\mu}_{e^-}(\Phi, \mathrm{pH}). \quad (4)$$

The free energy difference yields an independent estimate of the absolute electrode potential of the SHE at pH= 0. The free energy difference is 0.41 eV which yields an absolute value of U_{SHE} of 4.44 V which corresponds exactly to the experimental value [8, 14–16, 74]. This good agreement is to a certain extent fortuitous given the small size of the simulations cell which leads to broad Gaussian distribution in the total energies with a width of 1.3 eV. Still this indicates that the simulation cell is large enough to capture the main features of the electrochemical interface between Pt(111) and an aqueous electrolyte.

VII. CONCLUSIONS

The electrochemical interface between Pt(111) electrode and an aqueous electrolyte has been addressed by ab initio molecular dynamics simulations. Thermodynamic equilibrium properties have been estimated from the corresponding mean values along the trajectories with a varying number of hydrogen atoms in the simulation cell. The absolute electrode potential has been determined from the mean value of the work function along the AIMD trajectories. In particular, the potential of zero charge (pzc) has been derived from the simulation of an ion-free water film on Pt(111).

At the pzc, a partial charge transfer occurs from the solvating water layer to the Pt electrode leading to a dipolar polarization distribution along the interface normal. The creation of the interface dipole is essential to understand the work function change from Pt(111) in vacuum to the Pt electrode covered by a film of an aqueous electrolyte. The partial charge transfer at the pzc is a feature that has been typically neglected within traditional electrochemistry which has rather focused on the arrangement of point charges and the orientation of solvent molecules. However, DFT studies show that the charge transfer at the interface is a dominant contribution to determine the pzc [10].

Upon adding ions to the aqueous film, the electrode potential becomes changed due to the formation of additional dipolar polarizations induced by the presence of the ions in the electrolyte and adsorbates on the electrode. According to our calculations, the presence of ions in the water film leads to the formation of an asymmetric dipolar distribution along the surface normal with respect to the uppermost surface layer. In contrast, adsorbates at the interface tend to create a symmetric polarization along the interface normal direction which only causes small work function changes.

Therefore, in order to reliably describe the electrochemical interface, the polarization distributions have to be reproduced in the calculations. This also means that the electric double layer can not be satisfactorily described by a classical molecular mechanics approach. Instead, quantum chemical approaches such as periodic density functional theory calculations that explicitly consider the electronic distribution need to be employed. Previously, there have been attempts to model an electrochemical interface based a charged slabs which require the introduction of a counter charge in order to ensure overall charge neutrality [30, 31, 69, 81–87]. We suggest that these models can be further improved by constructing a counter electrode with a charge distribution based on the polarization distribution derived from simulations with an explicit solvent which will allow a better quantum chemical description of electrochemical interfaces.

ACKNOWLEDGEMENT

This research has been supported by the German Research Foundation (DFG) through contract GR 1503/21-1 and by the Baden-Württemberg Foundation within the Network of Excellence Functional Nanostructures. The authors acknowledge the computer time supported by the state of Baden-Württemberg through the bwHPC project and the Germany Research Foundation (DFG) through grant number INST 40/467-1 FUGG.

[1] R. Schlögl, ChemSusChem **3**, 209 (2010).
[2] M. Bellini, M. Bevilacqua, M. Innocenti, A. Lavacchi, H. A. Miller, J. Filippi, A. Marchionni, W. Oberhauser, L. Wang, and F. Vizza, J. Electrochem. Soc. **161**, D3032 (2014).
[3] H. Helmholtz, Ann. Phys. **243**, 337 (1879).
[4] L. G. Gouy, J. Phys. **9**, 457 (1910).
[5] D. L. Chapman, Philos. Mag. Series 6 **25**, 475 (1913).

[6] O. Stern, Z. Elektrochem. Angew. P. **30**, 508 (1924).
[7] D. C. Grahame, Chem. Rev. **41**, 441 (1947).
[8] S. Trasatti, Electrochim. Acta **36**, 1659 (1991).
[9] W. Schmickler and E. Santos, *Interfacial electrochemistry*, 2nd ed. (Springer Berlin / Heidelberg, 2010).
[10] J. Huang, A. Malek, J. Zhang, and M. H. Eikerling, J. Phys. Chem. C **120**, 13587 (2016).
[11] J. Rossmeisl, E. Skúlason, M. E. Björketun, V. Tripkovic, and J. K. Nørskov, Chem. Phys. Lett. **466**, 68 (2008).
[12] A. Groß, F. Gossenberger, X. Lin, M. Naderian, S. Sakong, and T. Roman, J. Electrochem. Soc. **161**, E3015 (2014).
[13] N. G. Hörmann, M. Jäckle, F. Gossenberger, T. Roman, K. Forster-Tonigold, M. Naderian, S. Sakong, and A. Groß, J. Power Sources **275**, 531 (2015).
[14] S. Trasatti, J. Electroanal. Chem. **150**, 1 (1983).
[15] S. Trasatti, Pure. Appl. Chem. **58**, 955 (1986).
[16] S. Trasatti, Electrochim. Acta **35**, 269 (1990).
[17] Y. Gohda, S. Schnur, and A. Groß, Faraday Discuss. **140**, 233 (2008).
[18] K. Letchworth-Weaver and T. A. Arias, Phys. Rev. B **86**, 075140 (2012).
[19] S. Sakong, M. Naderian, K. Mathew, R. G. Hennig, and A. Groß, J. Chem. Phys. **142**, 234107 (2015).
[20] A. N. Frumkin and O. A. Petrii, Electrochim. Acta **20**, 347 (1975).
[21] G. A. Tsirlina, in *Interfacial Phenomena in Electrocatalysis*, Vol. 51, edited by C. G. Vayenas (Springer-Verlag New York, 2011) Chap. 2, pp. 107–158.
[22] V. Tripkovic, M. E. Björketun, E. Skúlason, and J. Rossmeisl, Phys. Rev. B **84**, 115452 (2011).
[23] S. Brimaud, J. Solla-Gullon, I. Weber, J. M. Feliu, and R. J. Behm, ChemElectroChem **1**, 1075 (2014).
[24] M. H. Hansen, C. Jin, K. S. Thygesen, and J. Rossmeisl, J. Phys. Chem. C **120**, 13485 (2016).
[25] M. H. Hansen and J. Rossmeisl, J. Phys. Chem. C **120**, 29135 (2016).
[26] I. Ledezma-Yanez, W. D. Z. Wallace, P. Sebastián-Pascual, V. Climent, J. M. Feliu, and M. T. M. Koper, Nature Energy **2**, 17031 (2017).
[27] T. Ikeshoji, M. Otani, I. Hamada, O. Sugino, Y. Morikawa, Y. Okamoto, Y. Qian, and I. Yagi, AIP Adv. **2**, 032182 (2012).
[28] S. Sakong, K. Forster-Tonigold, and A. Groß, J. Chem. Phys. **144**, 194701 (2016).
[29] J. Le, M. Iannuzzi, A. Cuesta, and J. Cheng, Phys. Rev. Lett. **119**, 016801 (2017).
[30] S. Schnur and A. Groß, New J. Phys. **11**, 125003 (2009).
[31] S. Schnur and A. Groß, Catal. Today **165**, 129 (2011).
[32] E. Skulason, G. S. Karlberg, J. Rossmeisl, T. Bligaard, J. Greeley, H. Jonsson, and J. K. Norskov, Phys. Chem. Chem. Phys. **9**, 3241 (2007).
[33] M. H. Hansen, A. Nilsson, and J. Rossmeisl, Phys. Chem. Chem. Phys. **19**, 23505 (2017).
[34] M. Tuckerman, K. Laasonen, M. Sprik, and M. Parrinello, J. Chem. Phys. **103**, 150 (1995).
[35] A. Serr and R. R. Netz, International Journal of Quantum Chemistry **106**, 2960 (2006).
[36] D. Marx, ChemPhysChem **7**, 1848 (2006).
[37] K. J. Tielrooij, R. L. A. Timmer, H. J. Bakker, and M. Bonn, Phys. Rev. Lett. **102**, 198303 (2009).
[38] G. Meraj, M. Naganathappa, and A. Chaudhari, International Journal of Quantum Chemistry **112**, 1439 (2012).
[39] S. Kale and J. Herzfeld, Angewandte Chemie International Edition **51**, 11029 (2012).
[40] N. Agmon, H. J. Bakker, R. K. Campen, R. H. Henchman, P. Pohl, S. Roke, M. Thämer, and A. Hassanali, Chem. Rev. **116**, 7642 (2016).
[41] M. Ceriotti, W. Fang, P. G. Kusalik, R. H. McKenzie, A. Michaelides, M. A. Morales, and T. E. Markland, Chemical Reviews **116**, 7529 (2016).
[42] G. Kresse and J. Furthmüller, Phys. Rev. B **54**, 11169 (1996).
[43] P. E. Blöchl, Phys. Rev. B **50**, 17953 (1994).
[44] B. Hammer, L. B. Hansen, and J. K. Nørskov, Phys. Rev. B **59**, 7413 (1999).
[45] S. Grimme, J. Antony, S. Ehrlich, and H. Krieg, J. Chem. Phys. **132**, 154104 (2010).
[46] S. Grimme, Wiley Interdiscip. Rev. Comput. Mol. Sci. **1**, 211 (2011).
[47] S. Grimme, A. Hansen, J. G. Brandenburg, and C. Bannwarth, Chem. Rev. **116**, 5105 (2016).
[48] K. Tonigold and A. Groß, J. Comput. Chem. **33**, 695 (2012).
[49] K. Forster-Tonigold and A. Groß, J. Chem. Phys. **141**, 064501 (2014).
[50] B. Koslowski, A. Tschetschetkin, N. Maurer, P. Ziemann, J. Kučera, and A. Groß, J. Phys. Chem. C **117**, 20060 (2013).
[51] S. Sakong and A. Groß, ACS Catal. **6**, 5575 (2016).
[52] G. Mercurio, E. R. McNellis, I. Martin, S. Hagen, F. Leyssner, S. Soubatch, J. Meyer, M. Wolf, P. Tegeder, F. S. Tautz, and K. Reuter, Phys. Rev. Lett. **104**, 036102 (2010).
[53] S. Sakong, J. M. Fischer, D. Mahlberg, R. J. Behm, and A. Groß, Electrocatalysis **8**, 530 (2017).
[54] T. A. Manz and D. S. Sholl, J. Chem. Theory Comput. **6**, 2455 (2010).
[55] T. A. Manz and D. S. Sholl, J. Chem. Theory Comput. **8**, 2844 (2012).
[56] T. A. Manz and N. G. Limas, RSC Adv. **6**, 47771 (2016).
[57] N. G. Limas and T. A. Manz, RSC Adv. **6**, 45727 (2016).
[58] R. Bader, *Atoms in Molecules: A Quantum Theory* (Oxford University Press, New York, 1990).
[59] G. Henkelman, A. Arnaldsson, and H. Jónsson, Comp. Mater. Sci. **36**, 354 (2006).
[60] E. Sanville, S. D. Kenny, R. Smith, and G. Henkelman, J. Comput. Chem. **28**, 899 (2007).
[61] W. Tang, E. Sanville, and G. Henkelman, J. Phys.: Condens. Matter **21**, 084204 (2009).
[62] M. Yu and D. R. Trinkle, J. Chem. Phys. **134**, 064111 (2011).
[63] G. Jerkiewicz, Electrocatalysis **1**, 179 (2010).
[64] P. Quaino, N. Luque, G. Soldano, R. Nazmutdinov, E. Santos, T. Roman, A. Lundin, A. Groß, and W. Schmickler, Electrochim. Acta **105**, 248 (2013).
[65] S. Sakong and A. Groß, Electrocatalysis **8**, 577 (2017).
[66] T. Roman and A. Groß, Catal. Today **202**, 183 (2013).
[67] N. M. Marković and P. N. Ross Jr., Surf. Sci. Rep. **45**, 117 (2002).
[68] J. Le, A. Cuesta, and J. Cheng, J. Electroanal. Chem. (2017), https://doi.org/10.1016/j.jelechem.2017.09.002.
[69] M. Otani and O. Sugino, Phys. Rev. B **73**, 115407 (2006).
[70] I. Hamada, O. Sugino, N. Bonnet, and M. Otani, Phys. Rev. B **88**, 155427 (2013).
[71] T. Roman and A. Groß, Phys. Rev. Lett. **110**, 156804 (2013).

[72] F. Gossenberger, T. Roman, K. Forster-Tonigold, and A. Groß, Beilstein J. Nanotechnol. **5**, 152 (2014).
[73] A. Groß, *Theoretical surface science : A microscopic perspective* (Springer-Verlag, 2003).
[74] A. Cuesta, Surf. Sci. **572**, 11 (2004).
[75] G. S. Karlberg, J. Rossmeisl, and J. K. Norskov, Phys. Chem. Chem. Phys. **9**, 5158 (2007).
[76] J. K. Nørskov, J. Rossmeisl, A. Logadottir, L. Lindqvist, J. R. Kitchin, T. Bligaard, and H. Jónsson, J. Phys. Chem. B **108**, 17886 (2004).
[77] F. Gossenberger, T. Roman, and A. Groß, Surf. Sci. **631**, 17 (2015).
[78] M. Nielsen, M. E. Björketun, M. H. Hansen, and J. Rossmeisl, Surf. Sci. **631**, 2 (2015).
[79] X. Lin, F. Gossenberger, and A. Groß, Industrial & Engineering Chemistry Research **55**, 11107 (2016).
[80] F. Gossenberger, T. Roman, and A. Groß, Electrochim. Acta **216**, 152 (2016).
[81] O. Sugino, I. Hamada, M. Otani, Y. Morikawa, T. Ikeshoji, and Y. Okamoto, Surf. Sci. **601**, 5237 (2007).
[82] M. Otani, I. Hamada, O. Sugino, Y. Morikawa, Y. Okamoto, and T. Ikeshoji, Phys. Chem. Chem. Phys. **10**, 3609 (2008).
[83] N. Bonnet, T. Morishita, O. Sugino, and M. Otani, Phys. Rev. Lett. **109**, 266101 (2012).
[84] O. Andreussi, I. Dabo, and N. Marzari, J. Chem. Phys. **136**, 064102 (2012).
[85] O. Andreussi and N. Marzari, Phys. Rev. B **90**, 245101 (2014).
[86] G. Fisicaro, L. Genovese, O. Andreussi, N. Marzari, and S. Goedecker, J. Chem. Phys. **144**, 014103 (2016).
[87] G. Fisicaro, L. Genovese, O. Andreussi, S. Mandal, N. N. Nair, N. Marzari, and S. Goedecker, J. Chem. Theory Comput. **13**, 3829 (2017).